N71-33413
NASA CR-121433

NEW MEXICO STATE UNIVERSITY
LAS CRUCES, NEW MEXICO

ADVANCED STUDY OF VIDEO SIGNAL PROCESSING IN LOW SIGNAL TO NOISE ENVIRONMENTS

By

Frank Carden
Robert Bowden

A Semi-Annual Progress Report

Submitted to

NATIONAL AERONAUTICAL SPACE ADMINISTRATION
WASHINGTON, D. C.

NASA RESEARCH GRANT NGR-32-003-037

Electrical Engineering Department
Communication Research Group

June - November 1970

ENGINEERING EXPERIMENT STATION

NEW
MEXICO
STATE
UNIVERSITY
LAS CRUCES, NEW MEXICO

ADVANCED STUDY OF VIDEO SIGNAL PROCESSING IN LOW SIGNAL TO NOISE ENVIRONMENTS

By

Frank Carden
Robert Bowden

A Semi-Annual Progress Report

Submitted to

NATIONAL AERONAUTICAL SPACE ADMINISTRATION
WASHINGTON, D. C.

NASA RESEARCH GRANT NGR-32-003-037

Electrical Engineering Department
Communication Research Group

June - November 1970

ENGINEERING
EXPERIMENT
STATION

ABSTRACT

This work investigates the behavior of a bandpass filter in the multi-filter phase lock loop when driven with a sinusoidal drive. Amplitude jumps which are found in only nonlinear systems, are shown to exist in the multi-filter phase lock loop, providing information to help in understanding the operation of the loop.

TABLE OF CONTENTS

TABLE OF CONTENTS, (Continued)

LIST OF FIGURES

LIST OF FIGURES, (Continued)

LIST OF SYMBOLS

CHAPTER I

INTRODUCTION

1.1 Background

The phase lock loop (PLL) has become more widely used as an FM demodulator in the last several years. This is due to the noise rejection properties and associated threshold extension the PLL exhibits. These properties are particularly useful in receiving signals from spacecraft where the transmitted power is limited.

The typical lowpass PLL will give little or no threshold improvement over the conventional FM discriminator when the information is concentrated at or near discreet frequencies such as encountered with TV video [1]. Basically what happens is that the lowpass PLL allows noise in the unused portion of the bandwidth to enter the loop thus lowering the loop signal to noise ratio. This problem is further compounded by the poorer tracking performance of the lowpass PLL when strong subcarriers occur in the upper part of the passband [2].

A logical solution to these problems is to design a PLL which has a loop frequency response that is a comb structure matching that of the information spectrum. A PLL of this type, called a multi-filter phase lock loop (M-PLL), is of necessity a more complicated device and correspondingly will have a more complicated response. This work will be concerned with describing the phenomena associated with the bandpass filters in the loop when driven by a sinusoid.

1.2 The Basic PLL

The typical PLL consists of the elements shown in Figure 1.1. The VCO (voltage controlled oscillator) is a constant amplitude oscillator that has an output frequency controlled by the input voltage. The phase detector produces a voltage related to the phase difference of the VCO output and the input signal, usually the phase detector is a multiplier and the output is the sine of the phase difference. The loop filter is a linear time-invariant network that gives the typical loop an overall lowpass response. This model of the PLL, called the IF or carrier model, is not of a form that is readily analyzed.

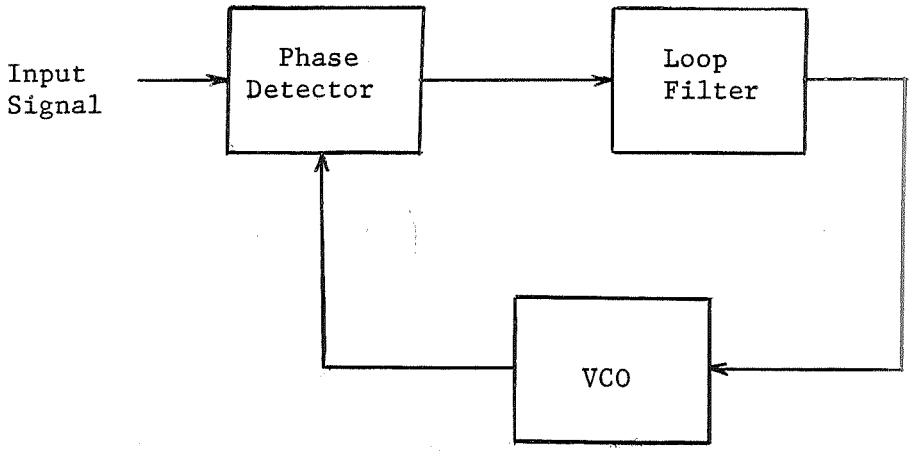

FIGURE 1.1 The Carrier Model of a PLL

Viterbi [3] has derived a reduced model, called the baseband or phase model, shown in Figure 1.2. This model is completely

described by the differential equation

$$(b_0 + b_1 \frac{d}{dt} + \cdots + b_n \frac{d^n}{dt^n})(\frac{d\phi(t)}{dt} - \frac{d\theta_i(t)}{dt})$$

$$= - AK(a_0 + a_1 \frac{d}{dt} + \cdots + a_m \frac{d^m}{dt^m}) \sin \phi(t), \qquad (1.1)$$

where the coefficients a_i and b_j are given by the s-domain transfer function of the loop filter.

$$F(s) = \frac{a_0 + a_1 s + \cdots + a_m s^m}{b_0 + b_1 s + \cdots + b_n s^n} \quad n \geq m \qquad (1.2)$$

Obviously (1.1) is nonlinear in terms of the dependent variable $\phi(t)$ and at this time there is no known exact solution. The lack of an exact solution will restrict the study of the PLL to special cases for which there are analytical methods. It is possible, however, to describe important phenomena of the PLL by making simplifying assumptions and thus reducing the problem of analyzing the loop performance to a manageable size.

1.3 Some Basic Assumptions

The most important and most restrictive assumption made in this study is that the filters are assumed non-interacting; that is, if a sinusoidal drive with frequency near the i^{th} bandpass filter is applied, the phase error, $\phi(t)$, will be due to the i^{th} bandpass filter only. This assumption is justified by arguing that the bandpass

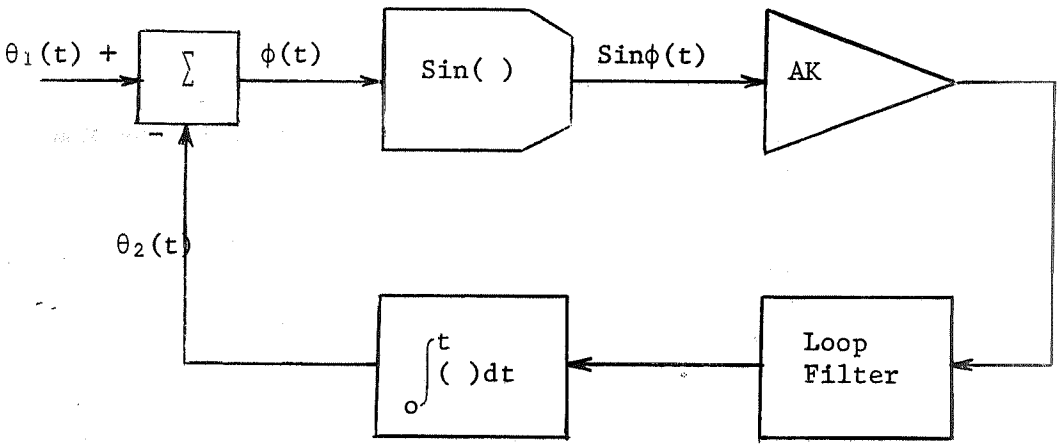

FIGURE 1.2 The Baseband Model of a PLL

filters are harmonically related and therefore, when the M-PLL is operating with the signal input for which it was designed, the harmonics due to the i^{th} filter will be small with respect to the inputs to the other filters. It is further assumed that the lowpass filter in the loop has no sinusoidal drive under normal operation; i.e. the lowpass filter will track only the carrier. The appendix gives the restrictions on the pole positions of the comb filters for the linear case.

The input signal will be assumed to be a single sinusoidal subcarrier in order that the phenomena associated with the bandpass filter may be explored. The response to this drive will be studied in the steady state.

As restrictive as these assumptions may seem, important phenomena such as amplitude jumps will be described.

CHAPTER II

A FIRST ORDER APPROXIMATION

2.1 The Loop Equation

The assumption that the filters are non-interacting reduces the equation describing the operation of the PLL considerably. With this assumption only the i^{th} bandpass filter need be considered. The bandpass filter will be assumed to have the form used by Cheng [4]. The s-domain transfer function for this bandpass filter is

$$F(s) = \frac{AK\ s^2}{s^2 + 2\zeta\ \omega_n\ s + \omega_n^2}\ . \tag{2.1}$$

The input is a single sinusoid modulated FM carrier given for the baseband model in (2.2), where $\Delta\omega$ is the frequency deviation and

$$\theta_1(t) = \frac{\Delta\omega}{\omega_m} \cos\ \omega_m t \tag{2.2}$$

ω_m is the modulating frequency. Substituting (2.1) and (2.2) into (1.1) the differential equation describing the PLL becomes

$$\ddot{\phi} + (2\zeta\ \omega_n + AK\ \cos\phi)\dot{\phi} + \omega_n^2\phi = \frac{\Delta\omega}{\omega_m}\ (\omega_m^2 - \omega_n^2)\ \cos(\omega_m t + \gamma)$$

$$+ \frac{\Delta\omega}{\omega_m}\ (2\zeta\ \omega_n\ \omega_m)\ \sin(\omega_m t + \gamma). \tag{2.3}$$

Equation (2.3)* has a first derivative term and therefore the solution will have a phase difference with respect to the driving function. In order to simplify the mathematics, the phase shift, γ, is associated with the driving function.

For a first order approximation the nonlinear term, cos ϕ, is replaced by the first two terms of its power series expansion. Equation (2.3) reduces to a form similar to the negative resistance oscillator problem [5].

$$\ddot{\phi} + \alpha(1 - \beta\phi^2)\omega_n \dot{\phi} + \omega_n^2 \phi = G \sin(\omega_m t + \gamma'), \tag{2.4a}$$

where

$$\alpha = 2\zeta + \frac{AK}{\omega_n}, \tag{2.4b}$$

$$\beta = \frac{AK}{2(2\zeta \omega_n + AK)}, \tag{2.4c}$$

$$G = \frac{\Delta\omega}{\omega_m} [(\omega_m^2 - \omega_n^2)^2 + (2\zeta \omega_n \omega_m)^2]^{\frac{1}{2}}, \tag{2.4d}$$

$$\gamma' = \text{ARCTAN} \left(\frac{2\zeta \omega_n \omega_m}{\omega_m^2 - \omega_n^2}\right) + \gamma . \tag{2.4e}$$

2.2 The First Harmonic Term

The steady state solution to this equation will be a function of the drive term. It is not unreasonable to expect that the

---

* The time dependence of $\phi(t)$ will be understood and here after will be written simply as ϕ.

response will be essentially sinusoidal if the parameter α is small compared to unity and if the parameter β is less than one. The approximate solution to (2.4a) might be expected to be of the form

$$\phi = E \cos \omega_m t \ . \tag{2.5}$$

The unknown quantities are the response amplitude, E, and the phase shift, γ'. These unknowns are found by applying the principle of harmonic balance; that is, with the assumed solution, the unknowns are forced to fit as well as possible.

Equation (2.5) is substituted into (2.4a) and the coefficients of the corresponding sine and cosine terms are collected, resulting in the following three relations.

$$\cos \omega_m t: \quad E(\omega_n^2 - \omega_m^2) = G \cos \gamma' \tag{2.6}$$

$$\sin \omega_m t: \quad -\alpha \omega_n \omega_m E\left(1 - \frac{\beta E^2}{4}\right) = G \sin \gamma' \tag{2.7}$$

$$\sin 3\omega_m t: \quad \alpha \omega_n \omega_m \frac{\beta E^3}{4} = 0$$

For this solution the third harmonic term will be neglected. The amplitude of the response may be found by squaring (2.6) and (2.7) and summing to eliminate the phase shift terms.

$$E^2\left[(\omega_n^2 - \omega_m^2) + (\alpha \omega_n \omega_m)^2\left(1 - \frac{\beta E^2}{4}\right)^2\right] = G^2 \tag{2.8}$$

This equation may be reduced by dividing by $(\alpha \omega_n \omega_m)^2$ and introducing the parameters

$$x = \frac{(\omega_n^2 - \omega_m^2)}{\alpha\, \omega_n\, \omega_m} , \tag{2.9}$$

$$y = \frac{\beta E^2}{4} , \tag{2.10}$$

$$A^2 = \frac{\beta G^2}{4(\alpha\, \omega_n\, \omega_m)^2} . \tag{2.11}$$

Upon carrying out the substitutions, (2.8) reduces to

$$y[x^2 + (1 - y)^2] = A^2 . \tag{2.12}$$

Equation (2.12) is cubic in terms of y and thus, there will always be one real solution to y for every x and A. There may also be three real solutions to y implying that jump phenomena may exist. The jumps will occur when $dy/dx = \infty$ or more simply $dx/dy = 0$. Upon carrying out the indicated derivative of (2.12) it is found that the jumps will occur along the ellipse

$$x^2 + 3\left(y - \frac{2}{3}\right)^2 = \frac{1}{3} . \tag{2.13}$$

A plot of (2.12) and (2.13) is shown in Figure 2.1. The parameter for the family of curves is A^2, which is proportional to the square of the drive amplitude and inversely proportional to the modulating frequency. If A^2 is less than 4/27 or greater than 8/27 there will be no jumps. Note, however, that the nonlinearity was approximated only by the first two terms of its power series expansion, and it is reasonable to expect more jumps than are predicted

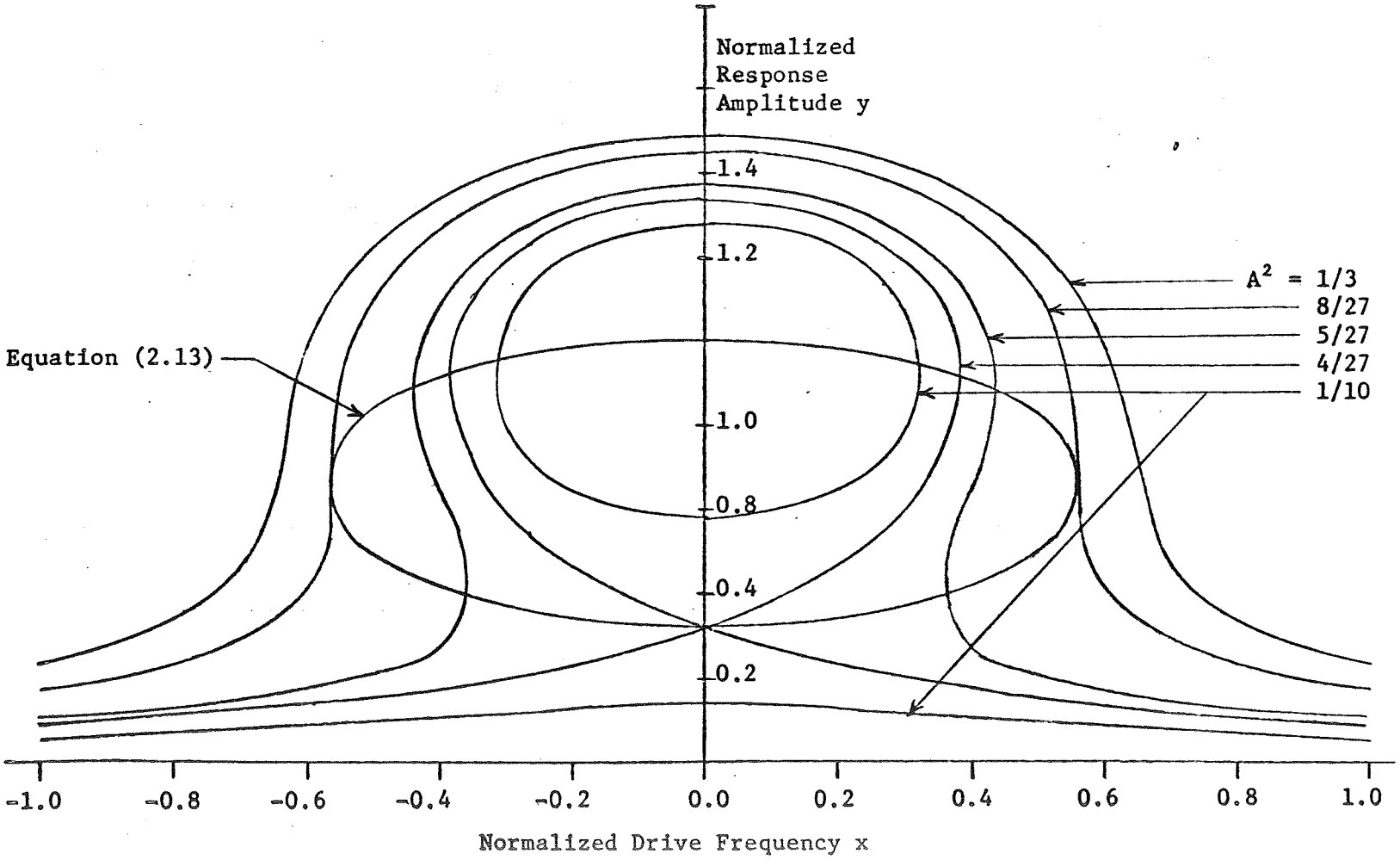

FIGURE 2.1 Normalized Response Curves of the M-PLL for Constant Drive Amplitude, First Approximation

here. A check of stability shows that the solution inside the ellipse are unstable and thus will not be observed in a physical system.

Another way of considering (2.12) is to hold the modulating frequency constant and vary the drive amplitude. As shown in Figure 2.2, an increase in A (modulation index) will result in an increase in E. At some point a small increase in A will result in a large jump in the response amplitude, E. After the jump has taken place A must be lowered until E jumps to a lower amplitude. This demonstrates a hysteresis effect in the response amplitude as well as the jump phenomena.

The normal operation of the PLL will require the phase error, ϕ, to be at a minimum. This corresponds to the parameter y being below the ellipse. From Figure 2.1 it is seen that for certain A's and x's, y will not meet this criterion. Therefore, it would be informative to have a plot relating the maximum A tolerable for a given x. Figure 2.3 is a plot of this boundary found by solving (2.12) and (2.13) along the lower edge of the ellipse and then denormalizing by using (2.11), (2.4d) and (2.4e). The particular case used was the same as used by Cheng [4]. Also plotted on this graph are the results found experimentally. The agreement is fair considering the approximation used for the nonlinearity and the assumed solution.

The phase shift term, γ', can be found by the proper manipulation of (2.12) and (2.6) along with the definitions of x, y, and A^2.

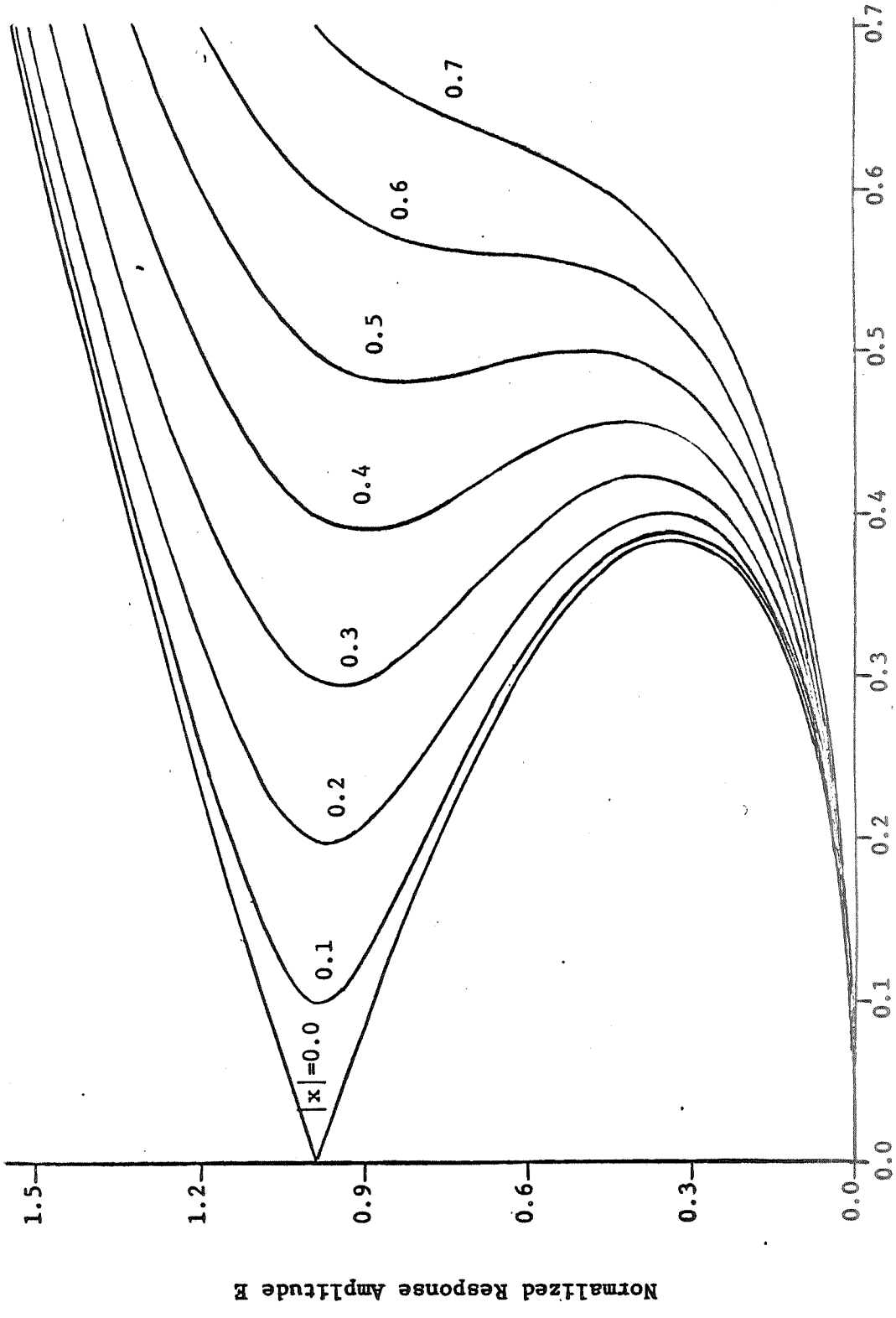

FIGURE 2.2 Normalized Response Curves of the M-PLL for Constant Frequency, First Approximation

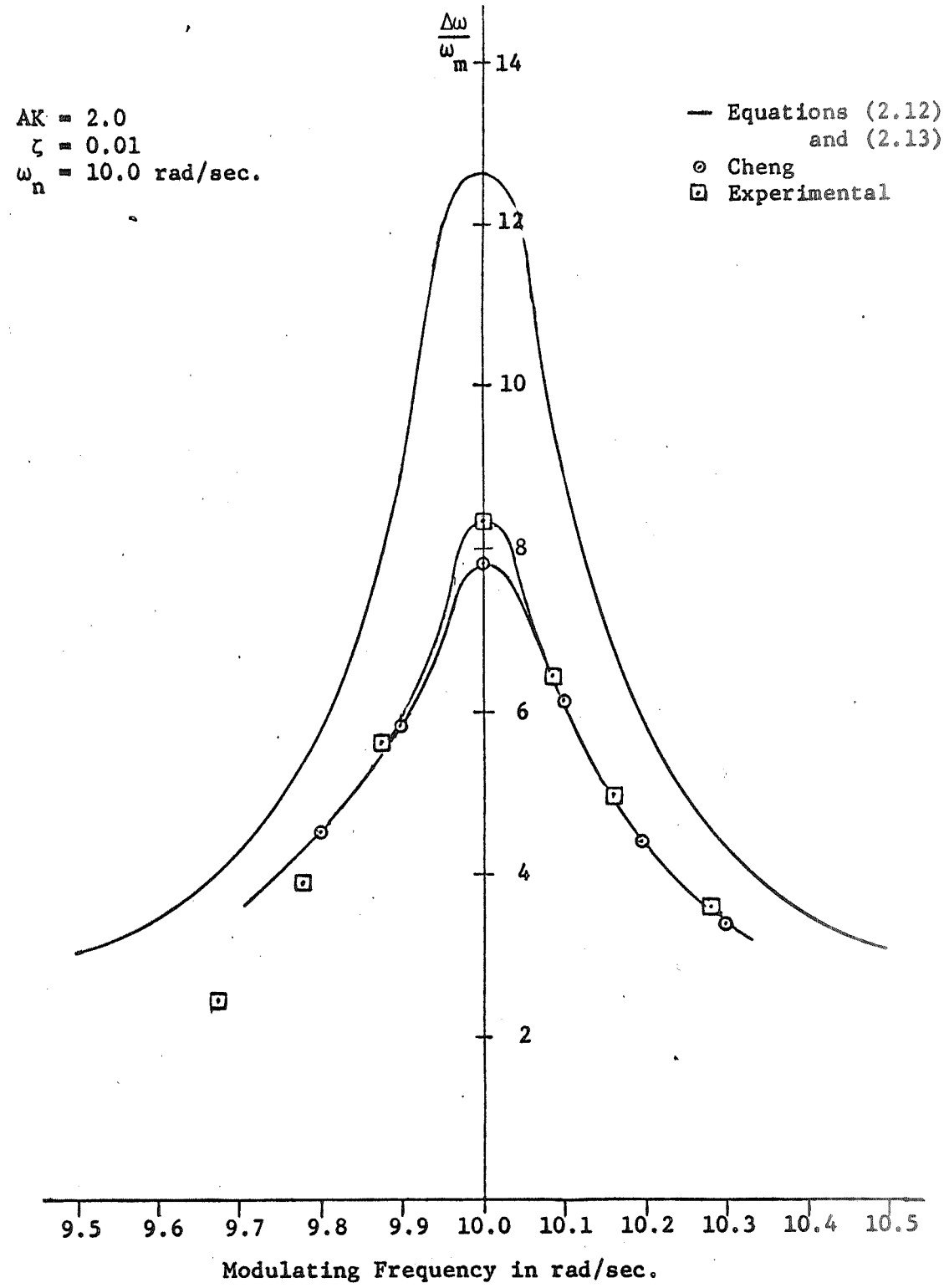

FIGURE 2.3 Boundary for First Response Jump, First Approximation

The phase angle, γ', is found to be

$$\text{TAN } \gamma' = \frac{x}{1 - y} . \tag{2.14}$$

The phase angle is plotted in Figure 2.4

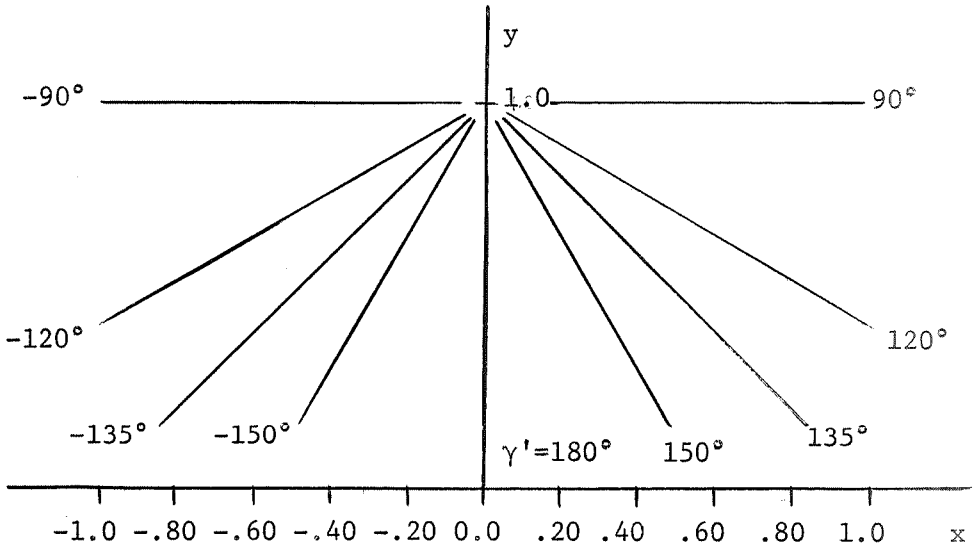

FIGURE 2.4 The Phase Angle of the Response, First Approximation

2.3 Discussion of Results

The response amplitude has been shown to exhibit jumps under the proper drive conditions. The input to the loop filter is the sine of the phase error and, after the jump has taken place, the peak phase error will be in the order of 2π. With the peak phase error this large the input to the loop filter will have large harmonic content and the assumed solution will not be valid. Furthermore the boundary for the first jump is not accurately predicted which implies that a more complicated solution must be considered.

The consideration of a more complicated solution will be deferred until the next chapter where a better model of the PLL is developed.

The jumps in the response amplitude may be observed in a M-PLL if care is used in the design. The jumps will involve larger phase error and larger phase error rate (frequency error) and, if due care in designing the PLL is not used, a component may saturate. This results in a loss of phase lock and may be misinterpreted as failure of the loop to track the modulation.

CHAPTER III

A SECOND APPROXIMATION

3.1 The Loop Equation

The first order approximation in Chapter II considered only the first two terms of the power series expansion for the cosine nonlinearity. If the nonlinearity is not approximated the results should be more accurate. The steady state solution to the PLL equation will be periodic and therefore will have a corresponding Fourier series of sine and cosine terms. Thus without an approximation of the cosine nonlinearity the solution will involve Bessel functions.

The equation describing the operation of the PLL under consideration was given in (2.3) as

$$\ddot{\phi} + (2\zeta\omega_n + AK\cos\phi)\,\dot{\phi} + \omega_n^2\phi = \frac{\Delta\omega}{\omega_m}(\omega_m^2-\omega_n^2)\cos(\omega_m t+\gamma) + \frac{\Delta\omega}{\omega_m}(2\zeta\omega_n\omega_m)\sin(\omega_m t+\gamma). \qquad (2.3)$$

This equation is simplified to

$$\ddot{\phi} + \alpha'(1+\beta'\cos\phi)\,\omega_n\dot{\phi} + \omega_n^2\phi = G\sin(\omega_m t+\gamma'), \qquad (3.1a)$$

where

$$\alpha' = 2\zeta, \qquad (3.1b)$$

$$\beta' = \frac{AK}{2\zeta\omega_n}, \qquad (3.1c)$$

$$G = \frac{\Delta\omega}{\omega_m}\left[(\omega_m^2-\omega_n^2)^2 + (2\zeta\omega_n\omega_m)^2\right]^{\frac{1}{2}}, \tag{3.1d}$$

$$\gamma' = \text{ARCTAN}\left(\frac{2\zeta\omega_n\omega_m}{\omega_m^2-\omega_n^2}\right) + \gamma. \tag{3.1e}$$

Note that there is not a one to one correspondence for α' and β' and α and β of Chapter II.

3.2 The First Harmonic Term

If $\alpha'<<1$ the first approximation for a steady state solution may be assumed to be

$$\phi = E \sin \omega_m t. \tag{3.2}$$

As before, the phase shift due to the damping term is associated with the driving function.

Substituting (3.2) into (3.1a) and collecting like sine and cosine term the following coefficient relations are found.

$$\cos \omega_m t: \quad \alpha'\omega_n\omega_m[E + 2\beta' J_1(E)] = G \sin \gamma' \tag{3.4}$$

$$\sin \omega_m t: \quad E(\omega_n^2-\omega_m^2) = G \cos \gamma' \tag{3.5}$$

The harmonic terms greater than one are neglected. The phase terms are eliminated by squaring (3.4) and (3.5) and summing the results.

$$E^2 (\omega_n^2-\omega_m^2)^2 + (\alpha'\omega_n\omega_m)^2 [E + 2\beta' J_1(E)]^2 = G^2 \tag{3.6}$$

This equation may be normalized by dividing by $(\alpha'\omega_n\omega_m)^2$. Thus

$$E^2x^2 + [E + 2\beta' J_1(E)]^2 = A^2, \tag{3.7a}$$

where

$$A = \frac{G}{\alpha' \omega_n \omega_m}, \tag{3.7b}$$

$$X = \frac{(\omega_n^2 - \omega_m^2)}{\alpha' \omega_n \omega_m}. \tag{3.7c}$$

Equation (3.7a) cannot be normalized in terms of E and therefore must be solved by use of graphical or numerical techniques. The arbitrary constant, β', in (3.7a) will have to be assumed and the solution will be for a specific case. The case chosen is the same as used by Cheng [4]. The plots in Figures 3.1 and 3.2 are curves for the solution where the parameter for the family of curves is x. Figure 3.2 is an expansion of Figure 3.1 for the region where the PLL will normally be used.

As in Chapter II a curve relating the maximum modulation index versus the modulating frequency for the first amplitude jump is of interest. The jumps in Figure 3.1 will occur when $dA/dE = \infty$ or $dE/dA = 0$; however, little is learned from the resultant derivative due to its complexity. Instead a graphical method is simpler: the values of x and A may be found from Figure 3.1 and denormalized using (3.1d), (3.7b), and (3.7c). This curve is plotted in Figure 3.3 along with the results from Chapter II.

These results, as with the results of Chapter II, do not agree exactly with experimental data leading to the conclusion that either the model or the assumed solution is incorrect. Experimental

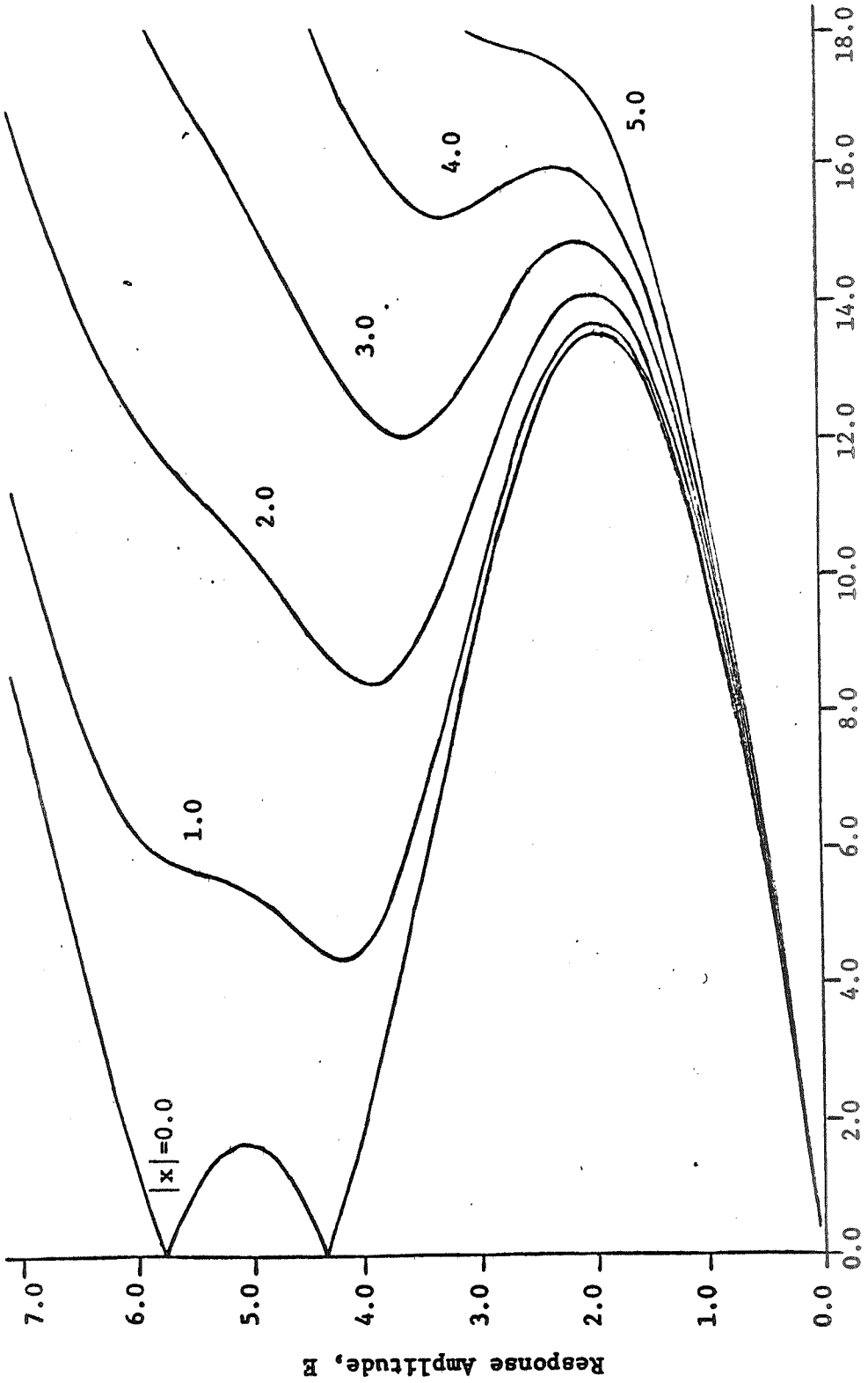

FIGURE 3.1 Normalized Response Curves of the M-PLL for Constant Drive Frequency, Second Approximation

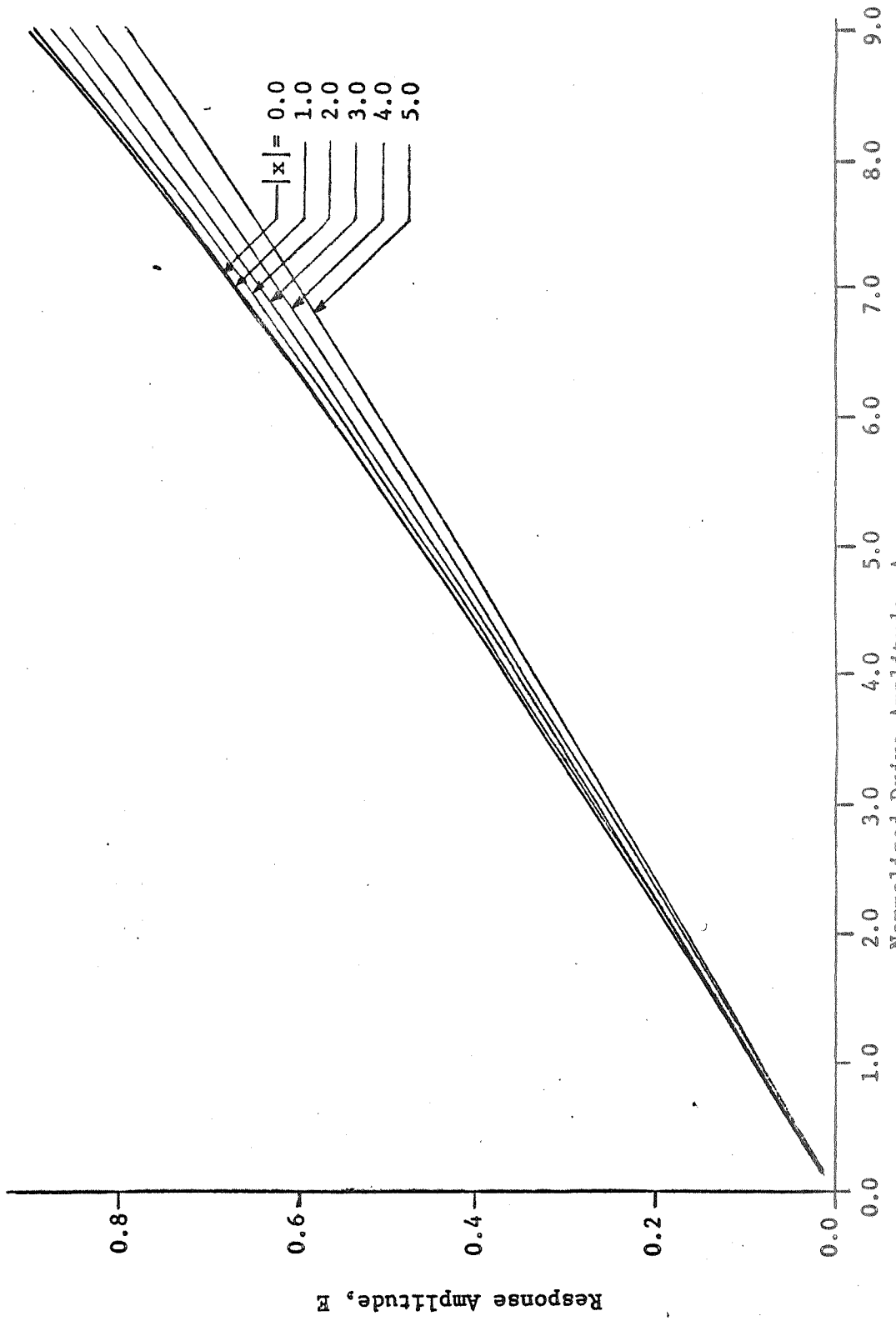

FIGURE 3.2 Response Curves for Typical Operating Region of the M-PLL for Constant Drive Frequency

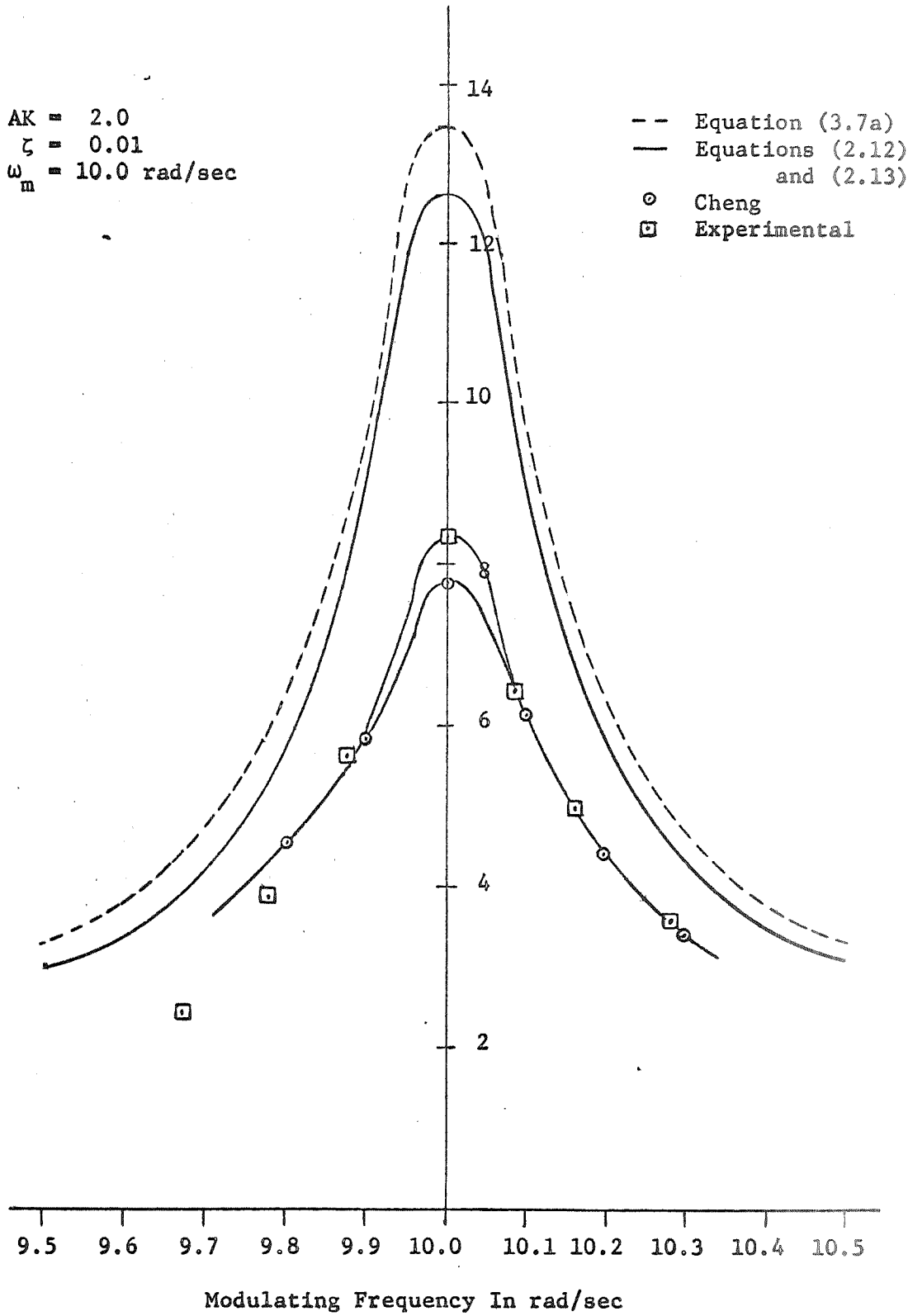

FIGURE 3.3 Boundary for First Response Jump, Second Approximation

observations of the M-PLL when operating slightly below the jump boundary indicate that the third harmonic term is large enough to be significant and should be considered.

This observation does not preclude the fact that the model may not be proper since the experimental model must include a lowpass loop for carrier tracking. If the difference in the jump boundary is caused by the neglect of the higher harmonic terms in the assumed solution, then the analytical predictions should agree with experimental results in operating regions where the higher harmonics may be neglected. This, of course, is the region of operation well below the jump boundary.

Again the case considered must be a specific case due to the nature of (3.7a). The results of the case used here are shown in Figure 3.4 along with the results found by Cheng [4]. The agreement is good; thus, it is concluded that the model used here is sufficient but higher harmonics must be considered if accurate jump boundaries are desired.

3.3 Higher Harmonic Terms

Before mentioning the form of the general steady state solution it is worthwhile to consider a special case. As will be seen, the consideration of more harmonic terms quickly leads to exceedingly complex solutions. Therefore, in an attempt to keep the mathematics in hand, only the first and third harmonic terms will be considered.

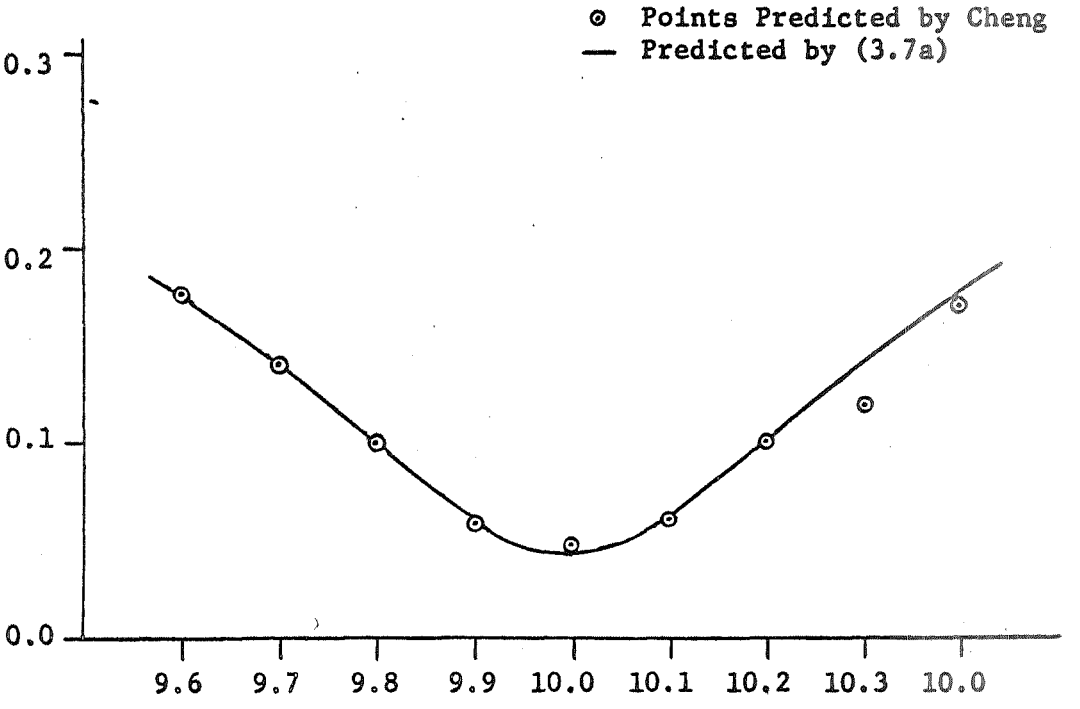

FIGURE 3.4 Comparison of Peak Phase Error as Predicted by Equation (3.7a) and by Cheng For the Bandpass Loop Where

$AK = 2.0$
$\zeta = 0.01$
$\omega_m = 10.0$ rad/sec

The assumed solution for (3.1a) becomes

$$\phi = E_1 \sin \omega_m t + E_3 \sin 3\omega_m t. \tag{3.8}$$

Substituting (3.8) into (3.1a) and collecting like sine and cosine terms the following coefficient equations result:

$$\cos \omega_m t: \quad \alpha'\omega_n\omega_m \{E_1 + \beta' \sum_{n=-\infty}^{\infty} J_n(E_3)[E_1(J_{-3n}(E_1)) + (\frac{E_1+3E_3}{2})$$

$$(J_{-(2+3n)}(E_1) + J_{(2-3n)}(E_1)) + \frac{3E_3}{2}(J_{-(4+3n)} + J_{(4-3n)}(E_1))]\}$$

$$= G \cos \gamma', \tag{3.9}$$

$$\sin \omega_m t: \quad E_1 (\omega_n^2-\omega_m^2) = G \sin \gamma', \tag{3.10}$$

$$\cos 3\omega_m t: \quad \alpha'\omega_n\omega_m \{3E_3 + \beta' \sum_{n=-\infty}^{\infty} J_n(E_3) [\frac{E_1}{2}(J_{(2-n)}(E_1) + J_{-(4+3n)}(E_1)$$

$$+ J_{(4-3n)}(E_1) + J_{-(2+3n)}(E_1)] + \frac{3E_3}{2}[2J_{-3n}(E_1)$$

$$+ J_{-3(2+n)}(E_1) + J_{3(2-n)}(E_1)]\} = 0, \tag{3.11}$$

$$\sin 3\omega_m t: \quad E_3 (\omega_n^2-9\omega_m^2) = 0. \tag{3.12}$$

These equations are exceedingly complex and the only possible way to solve them is with the use of a computer. Although no attempt was made at finding the E_1 and E_3 which satisfy these equations, the approach would be to square corresponding sine and cosine terms and to summing the results. This gives two equations in the two unknowns, E_1 and E_3. The difficulties in solving these two equations are left to the imagination of the reader.

The solutions quickly get out of hand because of the cosine

nonlinearity. In the general solution where all harmonics are considered, the substitution of the assumed solution into the cosine term will result in

$$\cos \left[\sum_{n=i}^{\infty} E_n \sin n\omega_m t \right].$$

This, of course, is the form of the multi-tone FM modulation for harmonically related tones and has not been satisfactorily solved to date.

3.4 Discussion of Results

The discrepancy between the analytically predicted jump boundary and the experimental boundary is larger than should be if the assumed solution is approximately correct. The implication is that the higher harmonics are large enough to require consideration. In a M-PLL these harmonics will cause distortion in the demodulated output; and therefore, the modulation index must be such that the PLL is operating well away from the boundary. For operation in this region (approximately that region shown in Figure 3.2) the operating parameters are accurately predicted by (3.7a).

CHAPTER IV

CONCLUSION

4.1 Summary

Jump phenomena in the response amplitude has been shown to exist in the bandpass filters of the M-PLL when the loop is excited with a sinusoidal drive. The jumps in the bandpass filters correspond to the jumps in the lowpass filter found by Stewart [6]. Hysteresis effects in the response amplitude have also been demonstrated.

The first order approximation in Chapter II predicts that only a single jump will take place; however, intuitive reasoning leads one to expect further amplitude jumps as can be found from (3.7a). Although the solutions do not accurately predict the points where the jumps occur, there is no reason to expect that the predicted jumps do not exist. The curves in Figures 2.2 and 3.1 also demonstrate a phenomena observed experimentally by Cheng. It was observed that the farther the modulating frequency was from the center frequency of the bandpass filter, the smaller the jump amplitude observed (Cheng refers to this as a lock to unlock transition).

Since the operation of the PLL near or past the point at which the first jumps occur will generate higher harmonics, the typical operating region will be approximately the region shown in Figure 3.2. This curve is generated from (3.7a) and, the phase error may be found by solving this equation to help in designing the loop.

4.2 Suggestions For Further Studies

Perhaps the most important problem yet to be studied is describing the operation of the M-PLL when two or more subcarriers compose the driving function. The most obvious technique to solve this problem would be to consider the energy in the loop. Unfortunately this method does not live up to expectations. This problem must be solved before a M-PLL can be designed with the assurance that it will operate properly.

Also of interest is the problem of signal distortion. Because the M-PLL will generate harmonics of the subcarriers, it would be informative to know the amplitude of the harmonics generated for the various loop parameters and the modulation index.

CHAPTER V

BIBLIOGRAPHY

(a) References Cited

[1] Carden, F. F., Thompson, W. E. and Cheng, E., "Multi-Filter Phase Lock Loop," IEEE Transaction on Communication Technology, to be published.

[2] Corl, Louis, "A Phase-Lock Loop Simulation and Its Behavior at Low Carrier to Noise Ratios," Master's Thesis, New Mexico State University, Las Cruces, New Mexico, 1969.

[3] Viterbi, A. J., Principles of Coherent Communications, McGraw-Hill Book Company, Inc., New York, 1966.

[4] Carden, F. F. and Cheng, E., "Advanced Study of Video Signal Processing in Low Signal to Noise Environments," Quarterly Progress Report, NASA Research Grant NGR-32-003-037.

[5] Cunningham, W. J., Introduction to Nonlinear Analysis, McGraw-Hill Book Company, Inc., New York, 1958.

[6] Stewart, I. A., "Some Solution and Stability Criteria for the Phase Lock Loop Equation," Master's Thesis, New Mexico State University, Las Cruces, New Mexico, 1970.

(b) Other References

[1] Truxal, J. G., Automatic Feedback Control System Synthesis, McGraw-Hill Book Company, Inc., New York, 1955.

[2] Stern, T. E., Theory of Nonlinear Networks and Systems, Addison-Wesley Publishing Company, Inc., Reading, Massachusetts, 1965.

[3] Hayashi, Chihiro, Nonlinear Oscillations in Physical Systems, McGraw-Hill Book Company, Inc., New York, 1964.

[4] Panter, P. F., Modulation, Noise, and Spectral Analysis, McGraw-Hill Book Company, Inc., New York, 1965.

[5] Gardner, F. M., Phase Lock Techniques, John Wiley and Sons, Inc., New York, 1966.

APPENDIX

APPENDIX

POLE LOCATIONS TO MINIMIZE FILTER INTERACTION FOR THE LINEAR PLL

To support the assumption that the filters are noninteracting, the pole positions of the filters in the loop must be independent. Independence of the pole positions will not only ease the analytical considerations but will also simplify the design of the M-PLL.

The comb filter is usually realized using delay lines as opposed to the use of many bandpass filters. When the comb filter of the delay line type is connected into the loop, the poles are not subject to individual movement. For this reason it is necessary to consider only the poles of the lowest bandpass filter and the poles of the lowpass filter.

Typically the lowpass response will be second order and the filter will have an s-domain transfer function of

$$F_L(s) = AK_L\left(1 + \frac{a}{s}\right). \tag{A.1}$$

The bandpass filter may be considered to have a transfer function given in Chapter II.

$$F_B(s) = \frac{AK_B S^2}{S^2 + 2\zeta_B \omega_{nB} S + \omega_{nB}^2} \tag{A.2}$$

The overall transfer function for the system will be

$$F_{(s)} = \frac{(AK_L+AK_B)s^3 + AK_L(2\zeta_B\omega_{nB}+a)s^2 + AK_L(\omega_{nB}^2+2a\zeta_B\omega_{nB})s + AK_L a\omega_{nB}^2}{s^3 + 2\zeta_B\omega_{nB}s^2 + \omega_{nB}^2 s} \tag{A.3}$$

The roots of the linear PLL may be found by substituting (A.1) into (1.1) where sin $\phi = \phi$ and finding the characteristic equation.

$$\lambda^4 + (2\zeta_B\omega_{nB}+AK_L+AK_B)\lambda^3 + (\omega_{nB}^2+2\zeta_B\omega_{nB}AK_L+aAK_L)\lambda^2$$

$$+ (AK_L\omega_{nB}^2+2\zeta_B\omega_{nB}aAK_L)\lambda + (a\omega_{nB}^2AK_L) = 0 \qquad (A.4)$$

The roots of the characteristic equation will be the same as the poles of the s-domain transfer function of the linear PLL.

The particular case used for this study will have a lowpass loop with a damping factor of $1/\sqrt{2}$ and a natural frequency of 1 rad/sec, thus

$$a = 1/\sqrt{2},$$

$$AK_L = \sqrt{2}.$$

Further, the open loop damping factor for the bandpass filter will be

$$\zeta_B = 0.01$$

The s-domain poles of the linear PLL may be studied for various values of AK_B and ω_{nB} by solving for the roots of (A.4).

Figure A.1 is the second quadrant of the s-plane, showing the pole positions as AK_B and ω_{nB} are varied. The region shown is where the lowpass poles have moved less than ten percent due to the influence of the bandpass poles.

When the poles of the bandpass filter are in the region indicated by Figure A.1, the results of this study are valid. It

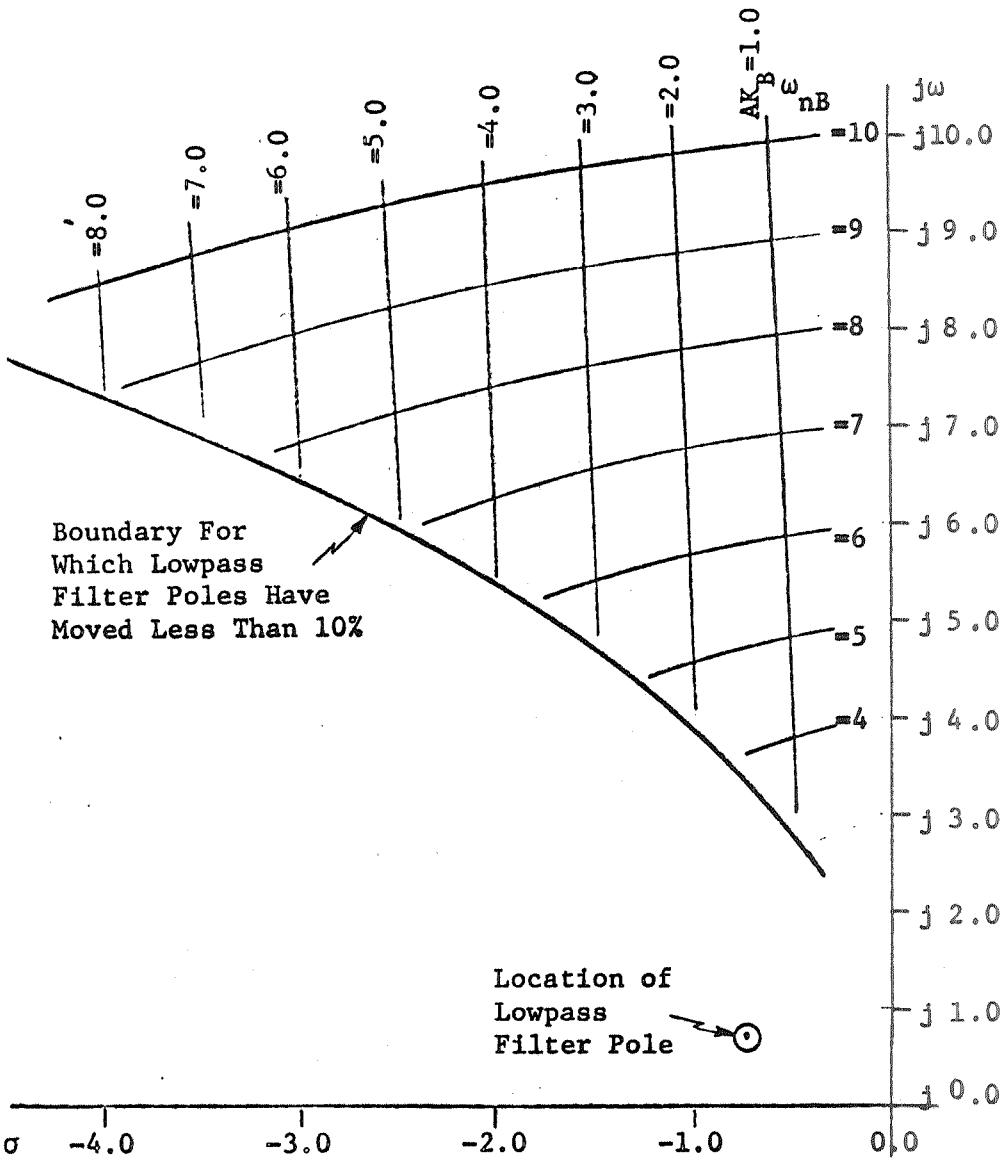

FIGURE A.1 Second Quadrant of s-plane for a Lowpass Filter and One Bandpass Filter

should be noted that with the poles in the region indicated, the stability of the loop is guaranteed. If the poles are moved closer together, the loop will eventually become unstable as shown in Figure A.2.

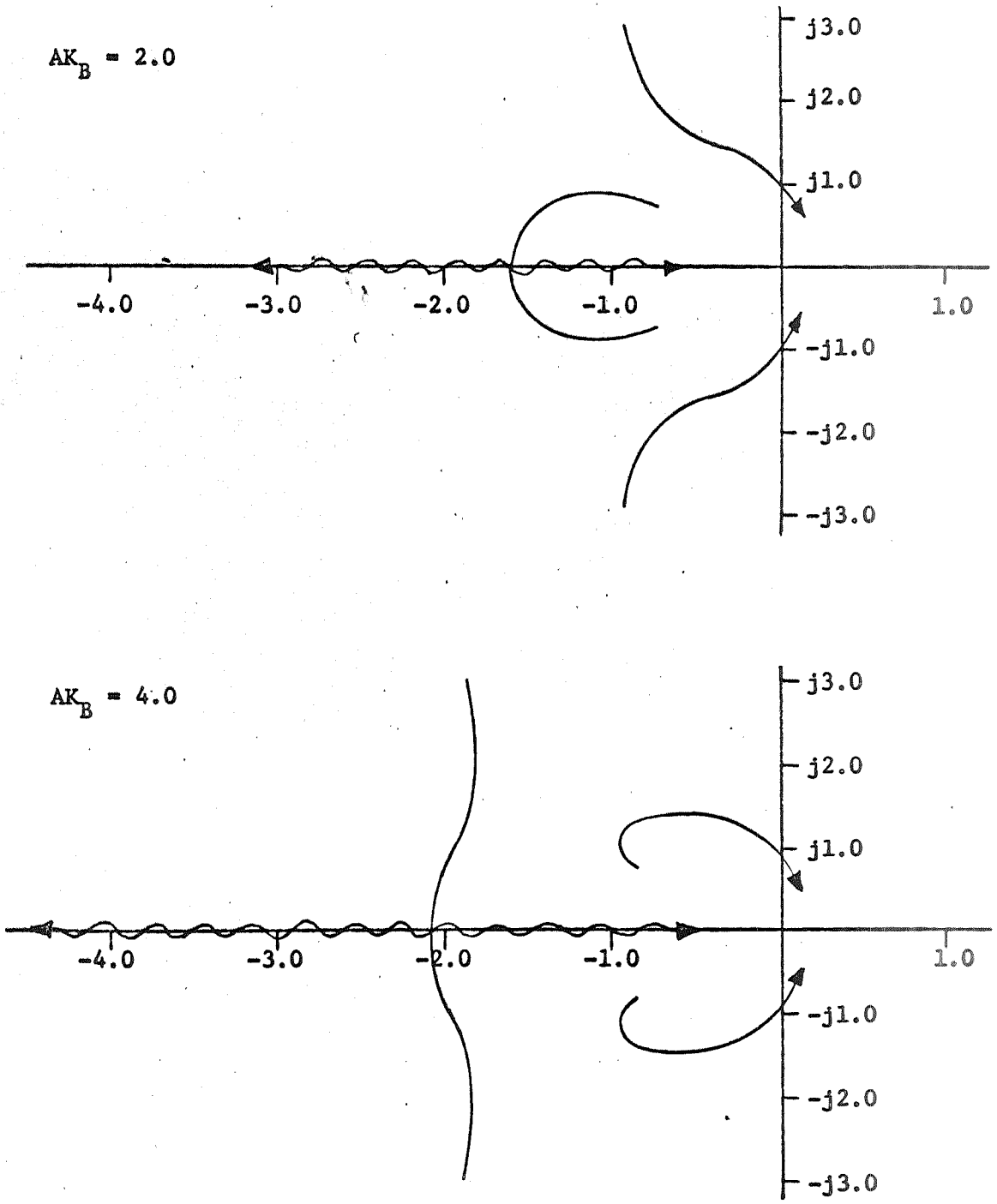

FIGURE A.2. Root Locus Plot for Linear M-PLL as ω_{nB} is Reduced to Zero